International Conference on Space Optics—ICSO 2022

Dubrovnik, Croatia

3–7 October 2022

Edited by Kyriaki Minoglou, Nikos Karafolas, and Bruno Cugny,

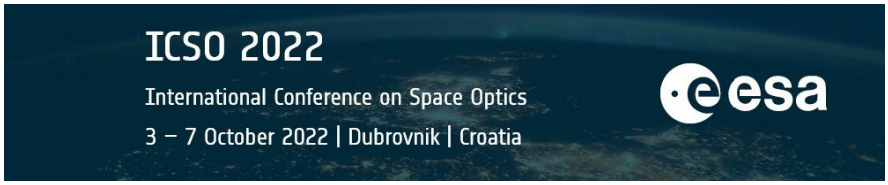

Interferometric imaging as an alternative to telescopes

International Conference on Space Optics — ICSO 2022, edited by Kyriaki Minoglou, Nikos Karafolas, Bruno Cugny, Proc. of SPIE Vol. 12777, 127770C · © 2023 ESA and CNES · 0277-786X · doi: 10.1117/12.2688803

Interferometric imaging as an alternative to telescopes

Hiyam Debary[a,c], Vincent Michau[a], Laurent Mugnier[a], Frédéric Cassaing[a], Matthieu Castelnau[b], and Sébastien Lopez[c]

[a]ONERA, Université de Paris-Saclay, 6 Chemin de la Vauve aux Granges, Palaiseau, France
[b]CNES, 18 avenue Edouard Belin, Toulouse, France
[c]Airbus Defence and Space, 31 Rue des Cosmonautes, 31402 Toulouse Cedex 4, France

ABSTRACT

A concept of optical interferometric imager was proposed by Lockheed-Martin in the early 2010s. In this concept, the aperture is paved by lenses. The optical signals collected by these lenses are combined in photonic integrated circuits, allowing the simultaneous measurement of the Fourier components of the observed object at a number of spatial frequencies. This concept allows one to consider a very significant reduction of the size of optical telescopes, e.g., for Earth observation. Indeed, the transverse dimension of a device based on this concept remains close to that of a telescope of the same resolution since the transverse size determines the spatial resolution. On the other hand, its size along the optical axis is much smaller than that of a conventional telescope.

After a quick description of this concept, its intrinsic performance will be analyzed. The field of this device, its spatial resolution, the spectral constraints imposed by the interferometric measurement will be presented. Based on these preliminary considerations, the noise on the measurement will be evaluated. The measurement noise will be compared to that obtained with a focal plane imaging instrument.

The geometry of combination of the signals collected by the lenses, or aperture configuration, is a key issue to minimize the size of the device and optimize the quality of the reconstructed image at a given spatial resolution. The literature proposes solutions leading to a partial frequency coverage. In this communication, solutions will be presented leading to a frequency coverage that is more suitable for applications such as Earth observation.

Keywords: Interferometry, Photonic integrated circuit, Earth observation, signal-to-noise ratio, spatial frequency coverage

1. INTRODUCTION

The innovative optical imaging system concept based on interferometry known as SPIDER*[1] could bring substantial gains in size and weight compared to a conventional focal plane imager by combining the following ideas:

- replace a focal plane imager by an interferometer which is illustrated Fig. 1a ;
- use the technology of PICs (*Photonic Integrated Circuit*) to realize in an extremely reduced thickness the functions of phase shifting, beam coupling, spectral dispersion and detection, as illustrated Fig. 1b.

The concept of SPIDER was presented in 2013,[1] by researchers at Lockheed-Martin, and several preliminary experimental demonstrations followed.[3,4]Several aspects of such a concept have been studied since then.[5–9] A Si_3N_4 PIC demonstrator with 12 baselines and 18 spectral channels dispersed by an *Arrayed Waveguide Grating* or AWG was then developed by Lockheed-Martin and UC Davis.[10] The experimental laboratory demonstration of the near-infrared SPIDER imager based on this PIC resulted in a publication in 2018,[2] which is the most comprehensive publication by these two teams.

Further author information: (Send correspondence to V. Michau or Hiyam Debary)
V. Michau: E-mail: vincent.michau@onera.fr, Telephone: +33 (0)6 84 53 24 62
H. Debary: E-mail: hiyam.debary@universite-paris-saclay.fr, Telephone: +33 (0)6 35 58 54 43
*SPIDER stands for Segmented Planar Imaging Detector for Electrooptical Reconnaissance.

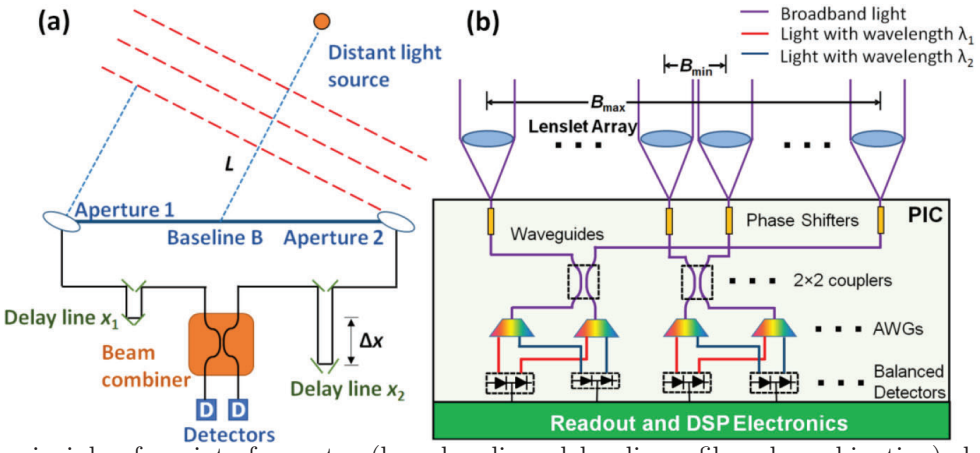

Figure 1: a: principle of an interferometer (long baseline, delay lines, fibered combination); b: principle of SPIDER (micro-lens array, injection in a PIC that contains phase shifters, couplers, dispersing elements (AWG) and detectors). Illustration taken from Ref. 2.

The diagram in Figure 1 shows that at their entry in the PIC, the beams in each guide meet first the phase shifters, then the couplers, which combine the apertures two by two, then only the dispersive elements (AWG), and finally the detectors. The flux recorded by the detectors allows, via a modulation produced by the phase shifters, to reconstruct the contrast and the phase of the interference fringes of each pair of recombined apertures. The contrast and phase are grouped into a quantity called *complex visibility*, which gives a sample of the Fourier Transform of the object via the Van Cittert-Zernike theorem. Then, the object can be estimated through an image reconstruction, using a method among those developed in astronomical interferometry.[11,12]

The telescope uses a large number of baselines to sample the complex visibility of the observed object on a rather large number of spatial frequencies. The implementation proposed by Lockheed-Martin is presented in Figure 2, taken from Ref. 2.

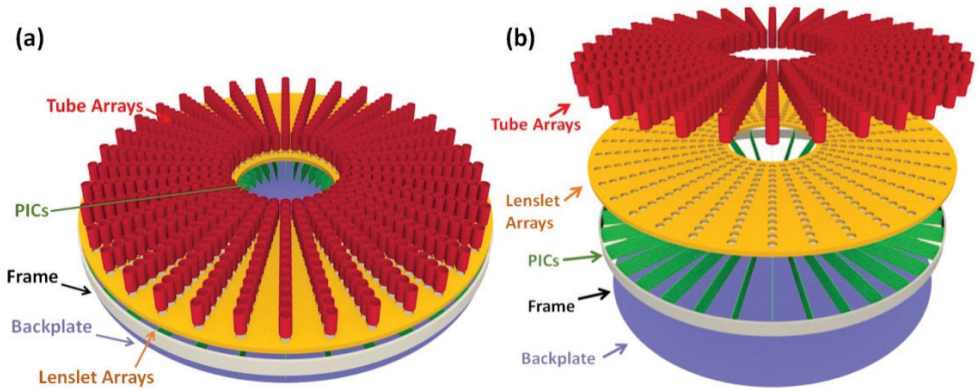

Figure 2: schematic diagram of a compact interferometric imager (taken from Ref. 2).

2. BASIC DESIGN RULES

2.1 Field of view

With SPIDER, the observed object is apodized by the "antenna lobe" in intensity L of the waveguide inside which the light is coupled, so that the effective object whose complex visibilities are measured by the interferometer is:

$$o_{\text{eff}}(\alpha_x, \alpha_y) = o(\alpha_x, \alpha_y) \times L(\alpha_x, \alpha_y). \quad (1)$$

L is the intensity of the back-propagation towards the object of the waveguide's propagation mode in the aperture plane: $L = |\mathrm{FT}(P)|^2$. L is typically a Gaussian 2D function of FWHM λ/D, where λ is the wavelength and D is the diameter of the apertures, as studied in details in Refs. 13,14. Finally, the field-of-view (FOV) of SPIDER is:

$$\theta_{\mathrm{fov}} = \lambda/D. \tag{2}$$

2.2 Visibility measurement model

Let us consider a pair of apertures separated by $\boldsymbol{B}$ measuring the spatial frequency $(u, v) = \boldsymbol{B}/\lambda$. Let us call C_1 (respectively C_2) the coupling coefficient of aperture 1 (respectively 2) towards the output, ϕ_k the modulation phase of the k-th measurement, and N_{ph} the mean number of photons received in each of the two apertures, during a given exposure time. Assuming balanced channels *i.e.*, $C_1 = C_2 = 1/\sqrt{2}$, a model of the recorded raw data (intensities) is:

$$i(u, v, \phi_k) = N_{\mathrm{ph}} \left\{1 + |\gamma(u, v)| \cos[\phi_k + \theta(u, v)]\right\}, \tag{3}$$

where the complex visibility of the observed object is:

$$\gamma(u, v) = |\gamma(u, v)| \exp(j\theta(u, v)) \ . \tag{4}$$

The mean number of photons received and detected per aperture and exposure time is:

$$N_{\mathrm{ph}} = \int o(\alpha_x, \alpha_y) \times L(\alpha_x, \alpha_y) \mathrm{d}\alpha_x \mathrm{d}\alpha_y \ . \tag{5}$$

By using typically four measurements ($\phi_k = (k-1)\pi/2$, for $k \in \{1, 2, 3, 4\}$) followed by a demodulation[†], one obtains a complex measurement $y(u, v)$ proportional to the mean number of photons received in each of the two apertures and to the complex visibility of the object at the measured spatial frequency:

$$y(u, v) = N_{\mathrm{ph}} \, |\gamma(u, v)| \exp(j\theta(u, v)) = N_{\mathrm{ph}} \gamma(u, v) \ . \tag{6}$$

Thanks to the Van Cittert-Zernike theorem:

$$\gamma(u, v) = \tilde{\boldsymbol{o}}_{\mathrm{eff}}(u, v) / \tilde{\boldsymbol{o}}_{\mathrm{eff}}(0, 0), \tag{7}$$

so $\gamma(0, 0) = 1$. Equation 6 then yields $y(0, 0) = N_{\mathrm{ph}}$, *i.e.*, the collection $\boldsymbol{y}$ of complex measurements $y(u, v)$ is a set of samples of the Fourier transform of $o_{\mathrm{eff}}(\alpha_x, \alpha_y)$ of integral (*i.e.*, of total flux) N_{ph}.

2.3 Resolution and number of resolution elements

As for any interferometer, the maximum spatial frequency recorded by a compact interferometric imager is given by the maximum distance separating two apertures, or maximum baseline $B_{\max}$, and is $B_{\max}/\lambda$. The angular resolution of such an instrument is thus:

$$r = \lambda / B_{\max} \ . \tag{8}$$

The angular field being λ/D, the number of resolved elements of a compact interferometric imager in the observable angular field is $B_{\max}/D$.

[†]For each spatial frequency (u, v), the demodulation consists in estimating $y(u, v)$ as: $\Re(y(u, v)) = (i(u, v, \phi_1) - i(u, v, \phi_3))/2$ and $\Im(y(u, v)) = (i(u, v, \phi_4) - i(u, v, \phi_2))/2$.

2.4 Spectral width

In case of point-like apertures separated by $\boldsymbol{B}$ interfering at a wavelength λ with zero bandwidth, the visibility is measured at the spatial frequency $\boldsymbol{B}/\lambda$. As soon as the bandwidth is non-zero, the detected interferogram is an average of inteferograms at the spatial frequencies given by all the wavelengths in the band. Therefore, what spectral bandwidth can be tolerated?

To answer this question, it is useful to realize that the recombined beams contain interferences between apertures of diameter D spaced by B and thus between pairs of points separated by distances ranging from $(B-D)$ to $(B+D)$. Such an interferometer with waveguide injection intrinsically measures an average of spatial frequencies of the object over a typical width of D/λ. It is then reasonable to specify that the spatial frequency averaging due to the spectral width $\mathrm{d}\lambda$ is less than the intrinsic averaging due to the non-zero aperture size. Differentiating $f = B/\lambda$ we obtain the following condition:[‡]

$$\mathrm{d}f = \frac{B}{\lambda^2}\mathrm{d}\lambda < D/\lambda.$$

For the shortest wavelength and the longest baseline, this yields:

$$\frac{\mathrm{d}\lambda}{\lambda_{\min}} < \frac{D}{B_{\max}}\,. \tag{9}$$

The inequality 9 can also be read as follows: the spectral resolution $\lambda/\mathrm{d}\lambda$ must be greater than the number of (spatially) resolved points of the interferometer, $B_{\max}/D$.

3. NOISE MODELING AND COMPARISON WITH A CONVENTIONAL IMAGER

A study of the compact interferometric imager concept must include the modeling of noise, and if possible comparatively to a classical *i.e.*, focal plane imager. The propagation of noise in the algorithm that reconstructs the object from complex visibilities is delicate because these algorithms can be notably non-linear. In order to avoid dealing with such noise propagation, we have chosen to model the noise of a compact interferometric imager and of a classical instrument in the Fourier *i.e.*, spatial frequency domain. An in-depth analysis may be found in.[15]

Here we assume that (only) two raw measurements are obtained simultaneously using the two outputs in phase opposition of each coupler. Two other measurements must then be obtained by introducing a phase shift of $\pi/2$. Each complex measurement thus uses $4N_{\mathrm{ph}}$ photons (2 raw interferometric measurements, each receiving N_{ph} photons per aperture). We assume in the following that the measurement noise is predominantly photon noise, which is reasonable for many scenarios at least in the visible and near-infrared. In the noise analysis, we additionally assume that the compact interferometric imager measures each spatial frequency only once, as in Ref. 16.

3.1 Noise modeling for a compact interferometric imager

Under the assumption that $|\gamma(u,v)| \ll 1$, the variance of the noise on the complex measurement $y(u,v)$ of Equation 6, resulting from the demodulation of four raw measurements given by Equation 3, is[§]:

$$\sigma_y^2(u,v) = N_{\mathrm{ph}}, \tag{10}$$

[‡]This condition can also be obtained by specifying that the optical path difference between two apertures separated by B for a direction $\theta = \lambda/(2D)$ at the edge of the field of view, which is $B.\theta = B\lambda/(2D)$, must be less than half the coherence length $L_c = \lambda^2/(\mathrm{d}\lambda)$.

[§]The variance of the complex variable y can be defined as $\mathrm{Var}(y) \triangleq E(|y - E(y)|^2)$, and it is easy to show that $\mathrm{Var}(y) = E(|y|^2) - |E(y)|^2 = \mathrm{Var}(\Re(y)) + \mathrm{Var}(\Im(y))$. If moreover, as we can reasonably assume in this study, $\Re(y)$ and $\Im(y)$ are two independent Gaussian variables of the same variance, then y is a complex circular Gaussian variable (distribution invariant by any rotation).

where N_{ph} is still the average number of photons received in each of the two apertures contributing to the interference during a raw measurement. This directly follows from the fact that $y(u,v)$ is the demodulation of 4 raw data measurements, where each is corrupted by photon noise, of variance N_{ph}.

The variance of these complex measurements, normalized by the square modulus of the signal at frequency (u,v), is therefore simply, according to Equation 5:

$$\frac{\sigma_y^2(u,v)}{|y(u,v)|^2} = \frac{N_{\text{ph}}}{N_{\text{ph}}^2|\gamma(u,v)|^2},$$

or:

$$\boxed{\frac{\sigma_y^2(u,v)}{|y(u,v)|^2} = \frac{1}{N_{\text{ph}}|\gamma(u,v)|^2}\,.} \tag{11}$$

3.2 Noise modeling for a conventional imager

The total number of elementary apertures of a compact interferometer SPIDER is denoted N_{d}. Considering each elementary aperture used a single time and connected by pairs, N_{d} is necessarily even and the number of measured spatial frequencies is $N_{\mathsf{d}}/2$. We consider an imaging system with the same collecting surface as this SPIDER[¶]. The object observed by the imaging system is assumed to be the object seen by the SPIDER device, $\boldsymbol{o}_{\text{eff}}$, to simplify the comparison. The measurement of each frequency requires the detection of 4 signals of average amplitude N_{ph}. The measurement of all these spatial frequencies therefore takes a total of $N_{\text{phtot}} = N_{\mathsf{d}}/2 \times 4N_{\text{ph}} = 2N_{\mathsf{d}}N_{\text{ph}}$ photons. Hence, the image model of a conventional imager collecting a total of N_{phtot} photons writes:

$$\boldsymbol{i} = 2N_{\mathsf{d}}.\boldsymbol{h} \star \boldsymbol{o}_{\text{eff}} + \boldsymbol{n}, \tag{12}$$

where $\boldsymbol{h}$ is the discrete PSF, and $\star$ is the discrete convolution operator.

We have already assumed that the visibility is negligible with regards to 1. For a classical imaging instrument, we additionally assume that the scene luminance is sufficiently homogeneous, so that the noise can be assumed to be stationary, *i.e.*, so that the variance of the noise of the classical imager σ_n^2 can be assumed to be approximately constant over all N_{pix} pixels. Hence, in the Fourier space, the noise spectrum is uniform and equals N_{phtot}.

Since $\tilde{\boldsymbol{o}}_{\text{eff}}(0,0) = N_{ph}$, as pointed out in paragraph 2.2, in the Fourier domain, the spectrum of the noise normalized by the square modulus of the signal at frequency (u,v) is:

$$\frac{\sigma_b^2(u,v)}{|\tilde{\boldsymbol{i}}(u,v)|^2} = \frac{N_{\text{phtot}}}{N_{\text{phtot}}^2|\gamma(u,v)|^2|\tilde{\boldsymbol{h}}|^2},$$

or:

$$\boxed{\frac{\sigma_b^2(u,v)}{|\tilde{\boldsymbol{i}}(u,v)|^2} = \frac{1}{2N_{\mathsf{d}} \times N_{\text{ph}}|\gamma(u,v)|^2|\tilde{\boldsymbol{h}}|^2}}\,. \tag{13}$$

Comparison of Equations 11 and 13 suggests that signal-to-noise ratios are similar for both types of instruments, *i.e.*, proportional to $\sqrt{N_{\text{ph}}}$, and that they are identical if:

$$|\tilde{\boldsymbol{h}}| = \frac{1}{\sqrt{2N_{\mathsf{d}}}}, \tag{14}$$

at all frequencies except the zero frequency, at which the MTF is 1 by convention. In other words, with respect to noise propagation, a "standard" compact interferometric imager (standard in the sense that each spatial frequency would be measured once and only once) is equivalent to a conventional imager with a flat MTF of the order of $\frac{1}{\sqrt{2N_{\mathsf{d}}}}$. Note that focal-plane imagers with quite flat MTFs exist, namely phased array instruments or sparse

[¶]The set of spatial frequencies to be measured to cover the same frequency support as a conventional imaging instrument of the same resolution, *i.e.*, of diameter $B_{\max}$, is contained in a half-disk of radius $B_{\max}/\lambda$, that is to say of the order of $\pi(B_{\max}/D)^2/2$ distinct frequencies, if the frequency sampling step is D/λ (which requires joint apertures).

aperture telescopes with minimal redundancy such as the ones discussed in Ref. 17. For these, the MTF is flat and of the order $1/N_{\text{tel}}$, where N_{tel} is the number of apertures.

Finally, the above results show that, for the highest spatial frequencies, a compact interferometric imager and a conventional imaging instrument have a very similar behavior with respect to noise. For the former, the propagation of noise is unfavorable for the lower frequencies. However it is quite possible, for a particular task (detection for example), to design the transfer function of a compact interferometric imager to make it higher at the spatial frequencies relevant to the task.

4. FREQUENCY COVERAGE

The set of measured spatial frequencies, *i.e.*, the *frequency coverage* is a key aspect in the design of the interferometer. Lockheed Martin's aperture configuration[18] of one arm is presented in the top panel of 3. The frequency coverage associated to this aperture configuration is presented at the bottom, and each measured frequency is represented by a blue dot. Since the spatial frequencies are sampled with a step of b/λ, with b the distance between two consecutive apertures, normalized spatial frequencies in units of b/λ are considered for simplicity purposes. Not all apertures are used (the unused ones are shown in red) and missing frequencies start from spatial frequency 7. The bidimensionnal optical transfer function deduced from this aperture configuration is illustrated in Fig. 6a.

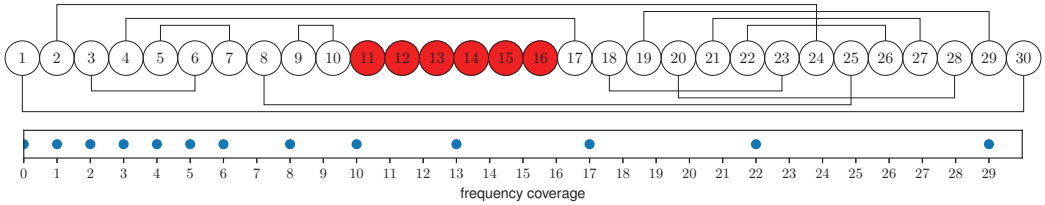

Figure 3: top panel: aperture configuration of an interferometric arm of the SPIDER-like instrument as described in;[18] the black lines represent aperture pairings; the unused apertures are colored in red - bottom panel: associated frequency coverage.

In case of the Earth observation viewed from a satellite, few priors are available making it necessary to have no gaps in the frequency coverage. A no gap frequency coverage is called compact.[19,20] Harvey and Rockwell[21] introduced the "practical resolution limit" (PRL), defining it as the maximum spatial frequency before which no zero occurs in the optical transfer function. In the following, the list of combined aperture pairs in the instrument is called *aperture configuration*. The monodimensional aperture configurations can be scanned to find the one with the highest PRL. Unfortunately, the number of aperture configurations scales exponentially with the number of apertures. An approach based on combinatorial theory results obtained by several authors[22–26] has been elaborated by Debary.[27] This paragraph summarizes her main results.

4.1 Optimization of the frequency coverage of dense 1D arrays

The total number of apertures in a single arm (1D) is denoted N_{p}. Still considering each aperture used a single time and connected by pairs, N_{p} is even. The number of measured spatial frequencies is consequently $N_{\mathsf{p}}/2$ and the measured frequencies have values in the range $[1, N_{\mathsf{p}} - 1]$.

A frequency coverage is defined as *buildable* if there is an aperture configuration that allows it to be measured (not all frequency coverages are buildable). Finding compact buildable frequency coverages composed of consecutive spatial frequencies $\{1, 2, \ldots, N_{\mathsf{p}}/2\}$ is a problem formulated and solved in the framework of combinatorial theory by Skolem.[23] Such a frequency coverage is called a Skolem set and its associated aperture configuration a Skolem sequence.

More generally, it is possible to build frequency coverages in the form $\{n_{\mathsf{min}}, n_{\mathsf{min}} + 1, \ldots, n_{\mathsf{min}} + N_{\mathsf{p}}/2 - 1\}$, where n_{min} is the first measured spatial frequency. This problem has been introduced by Langford.[28] Such a frequency coverage is called a Langford set and its associated aperture configuration a Langford sequence. The existence of buildable compact frequency coverages was proved for $n_{\mathsf{min}} = 1$ by Skolem in 1958, for $n_{\mathsf{min}} = 2$ by Davies[24] in 1959, then partially generalized by Bermond[25] in 1978 and finally completed by Simpson[26] in 1983.

4.2 Application to a SPIDER-like interferometer

Applying the Skolem results, an illustrative aperture configuration is provided in Fig. 4.

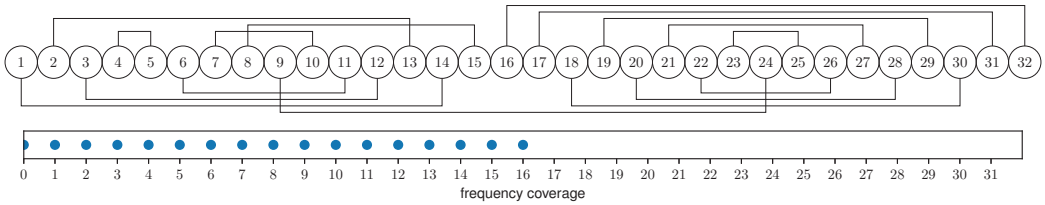

Figure 4: top panel: example of a Skolem aperture configuration with 32 apertures - bottom panel: associated normalized frequency coverage ranging from 1 up to 16.

4.3 Suggestion of a hybrid architecture using Langford configurations

It is possible to further optimize the PRL obtained for the SPIDER-like design by considering an interferometer based on a Langford sequence, complemented with a small monolithic telescope measuring short spatial frequencies.

If buildable, the Skolem configuration reaches a maximum spatial frequency of $N_\mathsf{p}/2$ by definition whereas the Langford configuration reaches a maximum spatial frequency of $(3N_\mathsf{p}-2)/4$. Because the maximum spatial frequency measured increases from $N_\mathsf{p}/2$ to $(3N_\mathsf{p}-2)/4$, the resolution of this hybrid interferometer is therefore improved by about 50% with respect to the interferometer with the Skolem configuration.

Maintaining the SPIDER-like interferometer aperture complexity, *i.e.* $N_\mathsf{p}=30$, an illustration of this Langford aperture configuration is presented in Fig. 5. The represented aperture configuration produces a compact frequency coverage ranging from spatial frequencies 8 to 22, improving the frequency coverage provided by a Skolem configuration, *i.e.* by considerably stretching the highest spatial frequency.

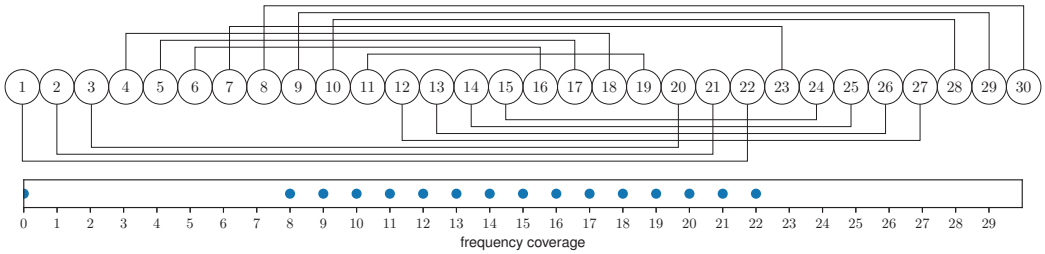

Figure 5: top panel: example of a Langford configuration with 30 apertures - bottom panel: associated frequency coverage ranging from spatial frequency 8 up to 22.

Finally, in Fig. 6b, we have represented the two-dimensional optical transfer function following the merging of the frequency coverages from the monolithic telescope and the SPIDER-like interferometer.

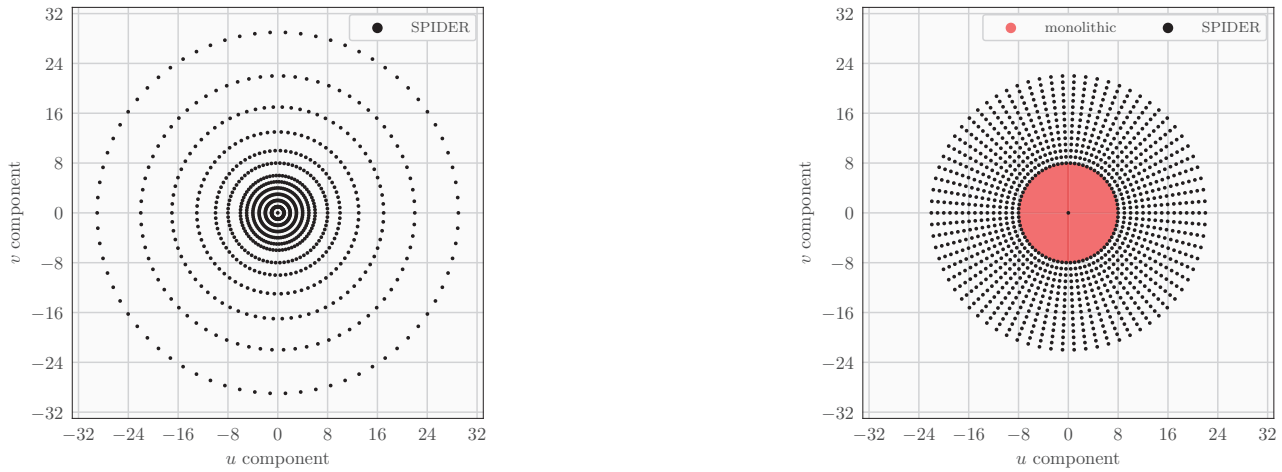

(a) (b)

Figure 6: optical transfer functions - a) SPIDER-like instrument with radially disposed arms, discrete spatial frequencies measured by the interferometer $\{1, 2, 3, 4, 5, 6, 8, 10, 13, 17, 22, 29\}$ (black) - b) suggested hybrid instrument: monolithic telescope complemented by SPIDER-like instrument with radially disposed arms, continuous spatial frequencies measured by the telescope $[1, 8]$ (red) and discrete spatial frequencies measured by the interferometer $\{8, \ldots, 22\}$ (black).

REFERENCES

[1] Kendrick, R. L., Duncan, A., Ogden, C., Wilm, J., and Thurman, S. T., "Segmented Planar Imaging Detector for EO Reconnaissance," in [*Imaging and Applied Optics*], CM4C.1, OSA, Arlington, Virginia (2013).

[2] Su, T., Liu, G., Badham, K. E., Thurman, S. T., Kendrick, R. L., Duncan, A., Wuchenich, D., Ogden, C., Chriqui, G., Feng, S., Chun, J., Lai, W., and Yoo, S. J. B., "Interferometric imaging using Si_3N_4 photonic integrated circuits for a SPIDER imager," *Optics Express* **26**, 12801–12812 (May 2018). Publisher: Optical Society of America.

[3] Scott, R. P., Su, T., Ogden, C., Thurman, S. T., Kendrick, R. L., Duncan, A., Yu, R., and Yoo, S. J. B., "Demonstration of a photonic integrated circuit for multi-baseline interferometric imaging," in [*2014 IEEE Photonics Conference*], 1–2 (Oct. 2014). ISSN: 1092-8081.

[4] Su, T., Scott, R. P., Ogden, C., Thurman, S. T., Kendrick, R. L., Duncan, A., Yu, R., and Yoo, S. J. B., "Experimental demonstration of interferometric imaging using photonic integrated circuits," *Optics Express* **25**, 12653 (May 2017).

[5] Liu, G., Wen, D.-S., and Song, Z.-X., "System design of an optical interferometer based on compressive sensing," *Monthly Notices of the Royal Astronomical Society* **478**, 2065–2073 (Aug. 2018).

[6] Gao, w., Wang, X., Ma, L., and Guo, D., "Quantitative analysis of imaging quality of the segmented planar imaging detector," in [*Tenth International Conference on Information Optics and Photonics*], Yang, Y., ed., 139, SPIE, Beijing, China (Nov. 2018).

[7] Guo-mian, L., Qi, L., Yue-ting, C., Hua-jun, F., Zhi-hai, X., and Jingjing, M., "An improved scheme and numerical simulation of segmented planar imaging detector for electro-optical reconnaissance," *Optical Review* **26**, 664–675 (Dec. 2019).

[8] Cao, K., Ye, Z., Jiang, C., Zhu, J., Qiao, Z., and Jiang, Y., "Lenslets combination optimal design of the segmented planar image detector for electro-optical reconnaissance," *Optical Engineering* **59**, 1 (Apr. 2020).

[9] Liu, G., Wen, D., Song, Z., and Jiang, T., "System design of an optical interferometer based on compressive sensing: an update," *Optics Express* **28**, 19349 (June 2020).

[10] Duncan, A., Kendrick, R., Ogden, C., Wuchenich, D., Thurman, S., Su, T., Lai, W., Chun, J., Li, S., Liu, G., et al., "Spider: next generation chip scale imaging sensor update," in [*Advanced Maui Optical and Space Surveillance Technologies Conference*], 6 (2016).

[11] Le Besnerais, G., Lacour, S., Mugnier, L. M., Thiébaut, E., Perrin, G., and Meimon, S., "Advanced imaging methods for long-baseline optical interferometry," *IEEE Journal of Selected Topics in Signal Processing* **2**, 767–780 (Oct. 2008).

[12] Thiébaut, E. and Young, J., "Principles of image reconstruction in optical interferometry: tutorial," *J. Opt. Soc. Am. A* **34**, 904–923 (June 2017).

[13] Dyer, S. D. and Christensen, D. A., "Pupil-size effects in fiber optic stellar interferometry," *JOSA A* **16**, 2275–2280 (Sept. 1999). Publisher: Optical Society of America.

[14] Mege, P., Malbet, F., and Chelli, A., "Interferometry with singlemode waveguide," in [*Interferometry for Optical Astronomy II*], **4838**, 329–337, International Society for Optics and Photonics (Feb. 2003).

[15] Mugnier, L. M., Michau, V., Debary, H., and Cassaing, F., "Analysis of a compact interferometric imager," in [*Space Telescopes and Instrumentation 2022: Optical, Infrared, and Millimeter Wave*], Coyle, L. E., Matsuura, S., and Perrin, M. D., eds., **12180**, Proc. Soc. Photo-Opt. Instrum. Eng. (2022). Conference date: July 2022, Montréal.

[16] Debary, H., Mugnier, L. M., Michau, V., and Lopez, S., "Optical interferometry imaging from space: optimization of the aperture configuration of a dense array," in [*Space Telescopes and Instrumentation 2022: Optical, Infrared, and Millimeter Wave*], Coyle, L. E., Matsuura, S., and Perrin, M. D., eds., **12180**, Proc. Soc. Photo-Opt. Instrum. Eng. (2022). Conference date: July 2022, Montréal.

[17] Cassaing, F. and Mugnier, L. M., "Optimal sparse apertures for phased-array imaging," *Opt. Lett.* **43**, 4655–4658 (Oct. 2018).

[18] Badham, K., Kendrick, R. L., Wuchenich, D., Ogden, C., Chriqui, G., Duncan, A., Thurman, S. T., Yoo, S. J. B., Su, T., Lai, W., Chun, J., Li, S., and Liu, G., "Photonic integrated circuit-based imaging system for spider," in [*2017 Conference on Lasers and Electro-Optics Pacific Rim (CLEO-PR)*], 1–5 (2017).

[19] Damé, L. and Martic, M., "Study of an optimized configuration for interferometric imaging of complex and extended solar structures.," *Targets for Space-Based Interferometry* **354**, 201–208 (1992).

[20] Mugnier, L. M., Rousset, G., and Cassaing, F., "Aperture configuration optimality criterion for phased arrays of optical telescopes," *J. Opt. Soc. Am. A* **13**, 2367–2374 (Dec 1996).

[21] Harvey, J. E. and Rockwell, R. A., "Performance characteristics of phased array and thinned aperture optical telescopes," *Optical Engineering* **27**(9), 279762 (1988).

[22] Nordh, G., "Perfect skolem sets," *Discrete mathematics* **308**(9), 1653–1664 (2008).

[23] Skolem, T., "Some remarks on the triple systems of steiner," *Mathematica Scandinavica* **6**(2), 273–280 (1958).

[24] Davies, R. O., "On langford's problem (ii)," *The Mathematical Gazette* **43**(346), 253–255 (1959).

[25] Bermond, J.-C., Brouwer, A. E., and Germa, A., "Systemes de triplets et differences associees," in [*Probèmes combinatoires et théorie des graphes, Colloque international CNRS 260*], **260**, 35–38, CNRS (1978).

[26] Simpson, J. E., "Langford sequences: perfect and hooked," *Discrete Mathematics* **44**(1), 97–104 (1983).

[27] Debary, H., Mugnier, L. M., and Michau, V., "Aperture configuration optimization for extended scene observation by an interferometric telescope," *Optics Letters* **47**(16), 4056–4059 (2022).

[28] Langford, C. D., "Langford problem," *Math. Gazette* **42**, 228 (1958).